bioRxiv preprint doi: https://doi.org/10.1101/520007; this version posted February 11, 2019. The copyright holder for this preprint (which was not certified by peer review) is the author/funder. All rights reserved. No reuse allowed without permission.

Ends and middle: global force balance determines septum location in fission yeast

Xavier Le Goff[1*], Jordi Comelles[2,3,4,5,6], Charles Kervrann[7] and Daniel Riveline[2,3,4,5,6*]

1 Univ Rennes, CNRS, IGDR (Institut de génétique et développement de Rennes) - UMR 6290, F- 35000 Rennes, France

2 Laboratory of Cell Physics ISIS/IGBMC, ISIS & icFRC, Université de Strasbourg & CNRS, 8 allée Gaspard Monge, Strasbourg 67000, France

3 Institut de Génétique et de Biologie Moléculaire et Cellulaire, Illkirch, France

4 Centre National de la Recherche Scientifique, UMR7104, Illkirch, France

5 Institut National de la Santé et de la Recherche Médicale, U964, Illkirch, France

6 Université de Strasbourg, Illkirch, France

7 SERPICO Team, INRIA Rennes, Campus de Beaulieu 35042 Rennes, France

*To whom correspondence should be addressed: xavier.le-goff@univ-rennes1.fr, riveline@unistra.fr

bioRxiv preprint doi: https://doi.org/10.1101/520007; this version posted February 11, 2019. The copyright holder for this preprint (which was not certified by peer review) is the author/funder. All rights reserved. No reuse allowed without permission.

Abstract

The fission yeast cell is shaped as a very regular cylinder ending by hemi-spheres at both cell ends. We proposed scaling arguments where the radii of curvatures of cell ends influence constraints on the cell wall. This relation predicts that the division site would be located closer to the cell end with the larger radius of curvature. By combining genetics and quantitative imaging, we tested experimentally whether altered shapes of cell end correlate with a displaced division site, leading to asymmetric cell division. Our results show that the division site position depends on the radius of curvatures of both ends.

Introduction

The fission yeast cell is shaped as a very regular cylinder ending by hemi-spheres at both cell ends. Fission yeast cells elongate during interphase keeping this regular shape, set by a balance between cell wall stiffness and turgor pressure (1). The cell is being remodelled locally at the cell ends to promote cell extension. The nucleus is permanently maintained in the middle of the cell by different forces, including microtubule pushing forces (2, 3). The central position of the nucleus is used as a spatial cue to assemble a contractile actomyosin ring when cells entered mitosis. This ring is used to drive the synthesis of a specific cell wall structure called the division septum, which physically separates the daughter cells into two cells. At this location, the cell wall undergoes a fracture, leaving two closed daughter cells approximately half the mother cell after cytokinesis. We proposed scaling arguments where the radii of curvatures of cell ends R_i influence constraints on the cell wall (1). They ultimately produce an effect on the division site position. This relation predicts that a higher radius of cell end curvature at one cell end should displace the division site by a length L_{shift} due to unbalanced strengths applied on the cell wall. The division site would be located closer to the cell end with the highest radius of curvature. We decided to test experimentally whether altered shapes of cell end actually correlate with a displaced division site, leading to an asymmetric cell division. We combined genetics together with live cell imaging. We used a constitutive deletion *tea4Δ* mutant and a conditional *kin1-as1* mutant, which affect cell ends. Our results show that the division site position depends on the radius of curvatures of both ends.

Results and Discussion

According to our scaling law, the cell end curvature would impact on cell division site position at the time of septum ingression due to cell wall constraints. Therefore, we monitored the cell division site localization using the expression of the cytokinetic ring component Cdc15-GFP (Figure 1A). Cellular outlines were stained with the cell wall isolectin-488 label. Equation 10 of reference (1) showed that this shift with actual center does not depend on the longitudinal cell length L (Figure 1B): $l_{shift} = (\gamma/(\Delta P \cdot R)) \cdot (R_1 - R_2)$, (Eq. 1), where R is the mean radius of the long axis, ΔP the constant difference in pressure between the inside and the outside of the cell and γ the cell wall surface tension.

bioRxiv preprint doi: https://doi.org/10.1101/520007; this version posted February 11, 2019. The copyright holder for this preprint (which was not certified by peer review) is the author/funder. All rights reserved. No reuse allowed without permission.

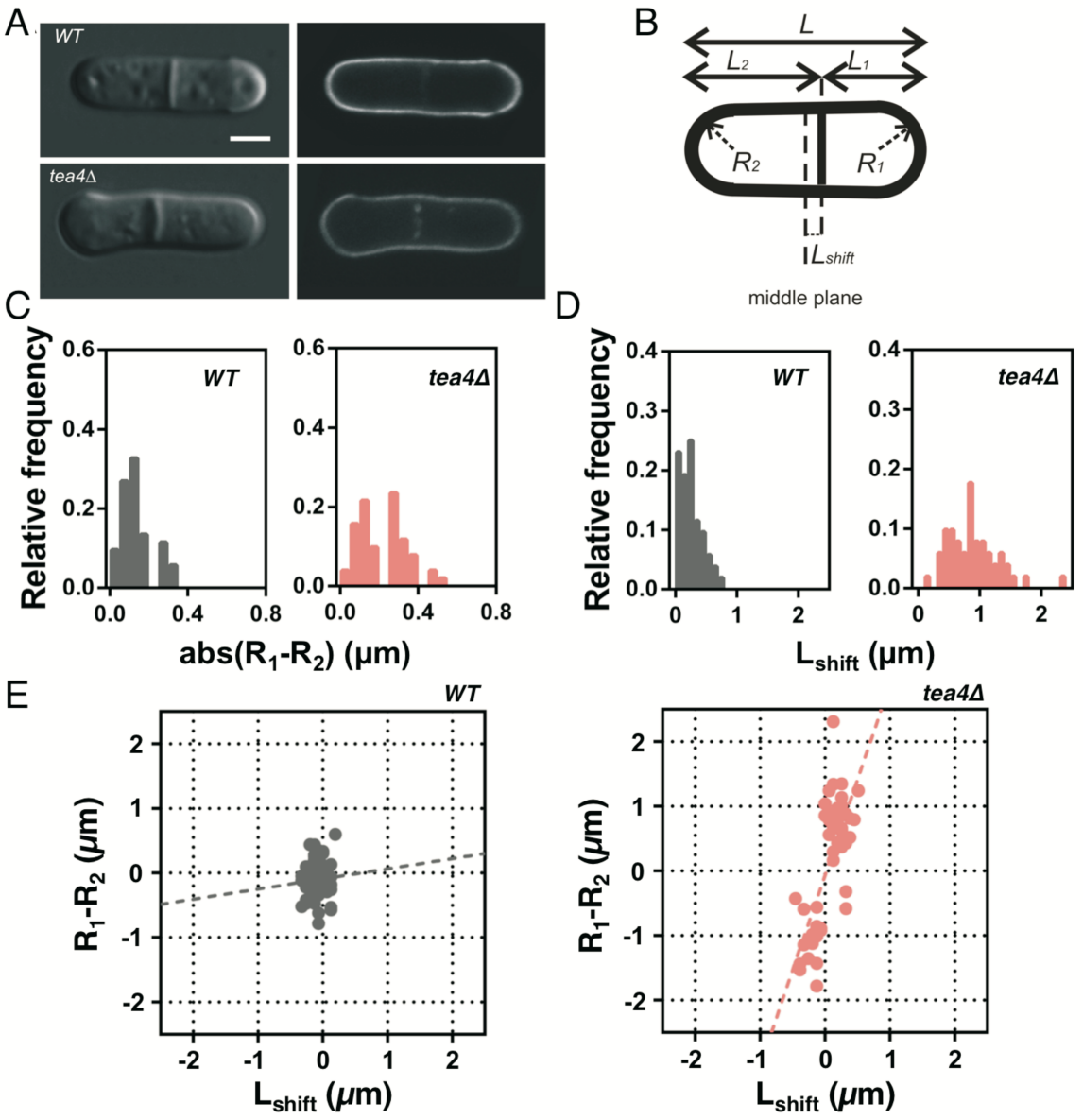

Figure 1. **(A)** DIC (left) and fluorescent (right) microscopy images (cdc15-GFP, isolectin-488) of WT and *tea4Δ*, Scale bar 2μm. **(B)** Schematics of the parameters measured in each cell: R_i corresponds to the radii of curvature at the cell "end i", and L_i corresponds to the distance between "end i" and septum; L_{shift} is defined as the distance between the septum and the middle plane ($L_{shift}=(L_2-L_1)/2$, L the total length). **(C)** Distributions of the absolute values of R_1-R_2 for the WT and *tea4Δ* cells. R_1-R_2 distributions are statistically different (t-test, $p = 0.0003$). **(D)** Distributions of the L_{shift} values for the WT and *tea4Δ* cells. Distributions are statistically different (Mann-Whitney, $p < 0.0001$). **(E)** Correlation between L_{shift} and R_1-R_2 for the WT and *tea4Δ* cells. The fits of Equation 1 are shown in the graphs. $n_{WT}=52$ and $n_{tea4\Delta}=51$. Pearson's correlation coefficients are 0.07 and 0.72 respectively.

First, we compared wild type (WT) and the asymmetrically dividing mutant *tea4Δ* (Figure 1A). The Tea4 protein is involved in bipolar activation of cell growth in the cell ends. *tea4Δ* cells showed altered cell morphology including one more enlarged cell end than the other and an asymmetrically positioned division site (4, 5). We measured cell end curvatures on both cell

bioRxiv preprint doi: https://doi.org/10.1101/520007; this version posted February 11, 2019. The copyright holder for this preprint (which was not certified by peer review) is the author/funder. All rights reserved. No reuse allowed without permission.

ends. Division site position was determined with Cdc15-GFP. The L_{shift} value was calculated as $L_{shift} = (L_2 - L_1)/2$ (Eq. 2) were L_1 stands for the shortest distance between the ring and one cell end (cell end1) and L_2 stands for the longest distance between the ring and the cell end (cell end2). To calculate the R_1-R_2 value, radii of curvatures were measured as follows: R_1 for cell end1 and R_2 for the other cell end. We observed an increased asymmetry in *tea4Δ* cells compared to WT, both for R_1-R_2 value (Figure 1C) and L_{shift} value (Figure 1D). On one hand, cell end radii are different in *tea4Δ* cells compared to WT cells. The difference of radii of cell end curvatures (R_1-R_2) slightly increased from 0.13±0.01 μm for WT cells to 0.21±0.02 μm for *tea4Δ* (Figure 1C). On the other hand, the mean value of L_{shift} increased from 0.26±0.05 μm for WT cells to 0.62±0.06 μm for *tea4Δ* cells (Figure 1D). There is clearly a larger amplitude of L_{shift} in *tea4Δ* cells indicating that they divide more asymmetrically than WT cells. Finally, the L_{shift}, plotted as a function of the R_1-R_2 difference of radii of cell end curvatures (Figure 1E), showed a positive correlation between L_{shift} and R_1-R_2 for *tea4Δ* cells (Pearson's correlation coefficient 0.72), whereas no correlation was observed for WT cells (Pearson's correlation coefficient 0.07). Therefore, the experimental results show that the division site is displaced towards the end with the highest radius of curvature, which is consistent with our prediction.

Tea4Δ cells are constitutively misshapen and cell end curvatures differences may arise from cell wall defects inherited through several generations independently of cell division site selection. Thus, we used *kin1-as1*, a conditional allele of the cell wall regulating Kin1 kinase, that promoted cell division site mispositioning within the duration of a cell division cycle. *Kin1-as1* was inhibited using a small molecule called NMPP1 added into the culture medium (6). *Kin1*$^-$ (*kin1-as1*+NMPP1) and *kin1*$^+$ (*kin1-as1*+DMSO) cells are isogenic but cultured with or without the inhibitor for 2 hours, respectively. *Kin1*$^-$ cells adopt an asymmetric cell division pattern in less than a generation time (see Figure 2A).

bioRxiv preprint doi: https://doi.org/10.1101/520007; this version posted February 11, 2019. The copyright holder for this preprint (which was not certified by peer review) is the author/funder. All rights reserved. No reuse allowed without permission.

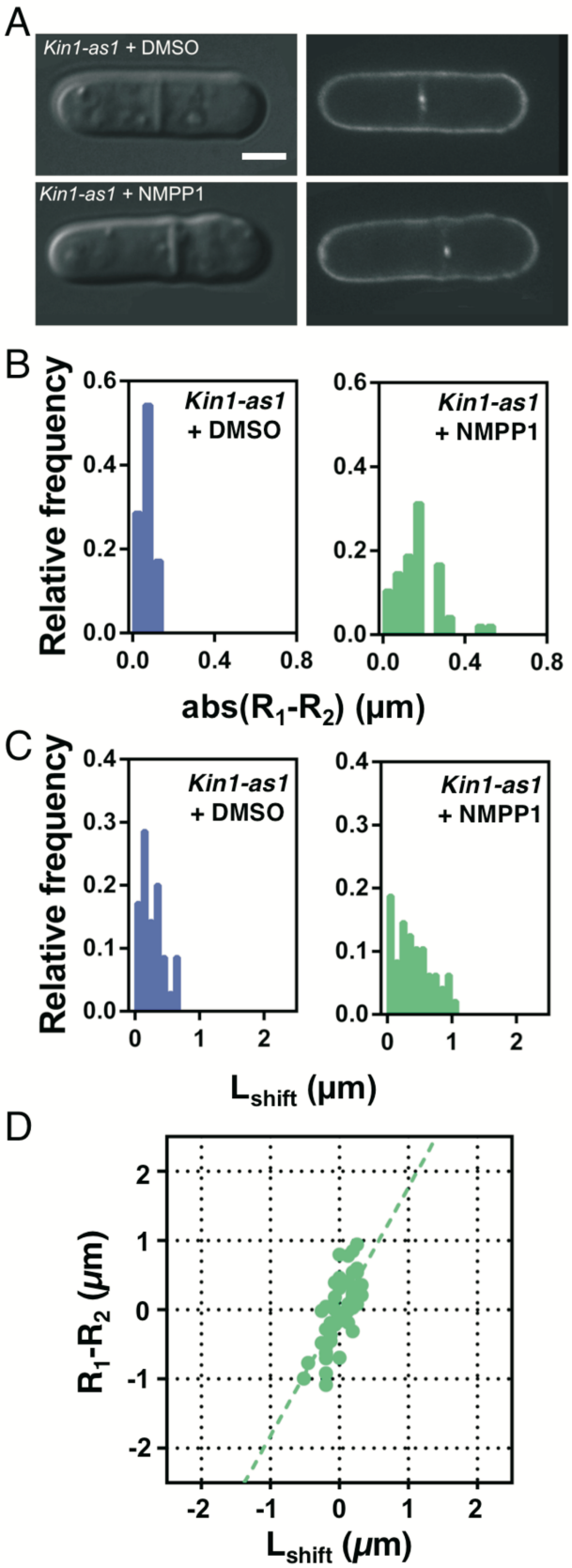

Figure 2. **(A)** DIC (left) and fluorescent (right) microscopy images (cdc15-GFP, isolectin-488) of *kin1-as1+DMSO and kin1-as1+NMPP1 cells*, Scale bar 2μm. **(B)** Distributions of the absolute values of R_1-R_2 for *kin1-as1+DMSO and kin1-as1+NMPP1* cells. R_1-R_2 distributions

bioRxiv preprint doi: https://doi.org/10.1101/520007; this version posted February 11, 2019. The copyright holder for this preprint (which was not certified by peer review) is the author/funder. All rights reserved. No reuse allowed without permission.

are statistically different (Mann-Whitney, $p < 0.0001$). **(C)** Distributions of the L_{shift} values for *kin1-as1+DMSO and kin1-as1+NMPP1* cells. Distributions are statistically different (t-test, $p = 0.0122$). **(D)** Correlation between L_{shift} and R_1-R_2 for *kin1-as1+NMPP1* cells. The fit of Equation 1 is shown in the graph. *51* $n_{Kin1\text{-}as1+DMSO}=35$ *and* $n_{Kin1\text{-}as1+NMPP1}=48$. Pearson's correlation coefficient is 0.72.

We monitored division site position and cell end curvatures using the method described above. R_1-R_2 value is higher in *kin1*$^-$ cells (0.17±0.02 µm) compared to *kin1*$^+$ cells (0.06 ±0.01 µm), showing that cell end radii are less equivalent (Figure 2B). Furthermore, a larger L_{shift} is clearly observed in *kin1*$^-$ cells (L_{shift} = 0.57±0.04 µm) compared to *kin1*$^+$ cells (L_{shift} = 0.25±0.02 µm) (Figure 2C). This indicates that *kin1*$^-$ cells divide more asymmetrically than DMSO treated cells and WT cells. Again, L_{shift}, plotted as a function of the R_1-R_2 (Figure 2D), showed a positive correlation between L_{shift} and R_1-R_2 for *kin1*$^-$ cells compared to *kin1*$^+$ cells (Pearson's correlation coefficient 0.72 and 0.44 respectively). L_{shift} was again displaced towards the end with the highest radius of curvature, confirming the results with the *tea4Δ* mutant and strongly supporting the scaling laws of paper (1). Based on these results, we could extract a quantitative estimate for the wall surface tension γ. Applying equation 1 and using the experimental values of L_{shift}, R_2, R_1 and R measured for *tea4Δ* cells (Figure 3A), we could obtain the distribution of the wall surface tension γ for each cell, assuming ΔP = 0.85 MPa (7) (Figure 3B). We then fitted the distribution with a gaussian function, obtaining a mean surface tension γ = 9.7±5.2 Nm, in good agreement with independent methods (7).

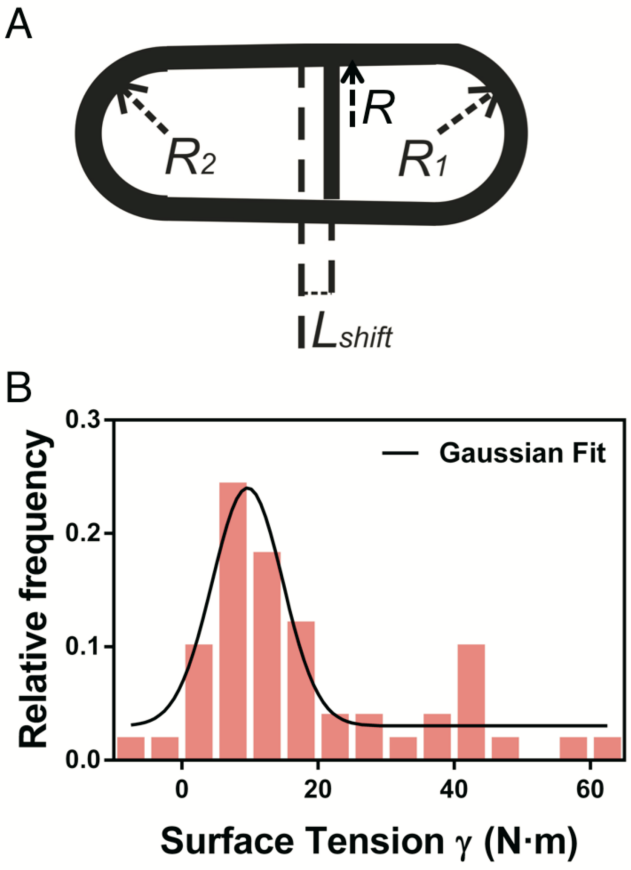

bioRxiv preprint doi: https://doi.org/10.1101/520007; this version posted February 11, 2019. The copyright holder for this preprint (which was not certified by peer review) is the author/funder. All rights reserved. No reuse allowed without permission.

Figure 3. (A) Schematics of the parameters used to obtain the surface tension γ for *tea4*Δ cells. **(B)** Distribution of surface tension γ for *tea4*Δ cells. γ was calculated according to Equation 1 assuming ΔP = 0.85 MPa (7). The data were fitted assuming a Gaussian distribution, obtaining a value for the surface tension of $\gamma = 9.7 \pm 5.2$ N·m.

Our results show that fission yeast cell end shapes influence the division site position. In WT cells, the small difference in both cell end radii promotes balanced global forces that place the division site close to the geometric cell center. Accordingly, daughter cells divide at nearly equal sizes and this might be crucial for cell population fitness regarding symmetric partitioning of cellular components and damaged material inheritance (8). We propose that two mechanisms contribute to symmetry of division in fission yeast: an 'external' input from cell wall driven forces and an 'internal' input driven by microtubule-dependent nuclear localization. In mutants where the cell wall synthesis machinery is depolarized from cell ends, the external cell wall contribution exceeds a threshold and cells divide asymmetrically, suggesting that the internal input cannot compensate the defect. The role of cell wall forces proposed here may be a generic mechanism in single celled symmetrically dividing organisms to produce equally sized daughter cells at each cell division.

Experimental procedures

Yeast Strains and General Techniques

S. pombe strains used in this study are XLG52 (*h- cdc15::GFP-ura4*$^+$ *ura4-D18 leu1-32*, a kind gift of V. Simanis, Switzerland), XLG540 (*h- tea4::ura4+ ura4-D18 cdc15::GFP-ura4*$^+$ *leu1-32*), XLG741 (*h- cdc15::GFP-ura4*$^+$ *kin1-as1 leu1-32 ura4-D18*). Growth media and basic techniques for *S. pombe* have been described (9).

Microscopy

A spinning disk Nikon TE2000 microscope, equipped with a 100x 1.45 NA PlanApo oil-immersion objective lens and a HQ2 Roper camera, was used for data acquisition. Cells expressed the acto-myosin ring component Cdc15-GFP and were stained 10 minutes with isolectin-488 (Molecular probes) that stains the global cell wall (but not the septum). Metamorph software was used for capturing images. The "three point circular" ImageJ Plugin allows to draw a ring with three points at a cell end and it gives the radius of curvature. We used this Plugin to measure radii of curvature to obtain the best measurements. Cell lengths (L, L_1 and L_2) were measured with the Plot profile Plugin.

Statistical analyses and graphical representation

Statistical analysis was done using GraphPad Prism. Results are presented as mean ± s.e.m of N = 3 experiments, n_{WT} = 52 cells, $n_{tea4\Delta}$ = 51 cells, $n_{kin1\text{-}as1+DMSO}$ = 35 cells and $n_{kin1\text{-}as1+NMPP1}$ = 48 cells. First, normality of the datasets was tested by the d'Agostino-Pearson normality test. Statistical differences were analyzed by t-test (Gaussian distribution) and Mann-Whitney test (non Gaussian distribution). The Pearson's r correlation coefficient was used in order to test the relation between (R_1-R_2) and L_{shift} for all the conditions. (R_1-R_2) as function of L_{shift} were fitted

bioRxiv preprint doi: https://doi.org/10.1101/520007; this version posted February 11, 2019. The copyright holder for this preprint (which was not certified by peer review) is the author/funder. All rights reserved. No reuse allowed without permission.

using a linear regression. To obtain the surface tension γ for *tea4*Δ cells, γ was calculated according to equation 1 assuming $\Delta P = 0.85$ MPa for every cell. The distribution of γ was plotted and fitted with a Gaussian distribution $y = y0 + A \cdot \exp(-(x-x_c)^2/(2 \cdot w^2))$, where x_c is the mean value for γ and w corresponds to the standard deviation.

Authors contributions

XLG and DR designed the research, analyzed the data and wrote the manuscript; XLG performed the cell experiments and image acquisition and analyses; JC performed the statistical analyses and manuscript figures; CK helped in image processing. Correspondence should be addressed to XLG (xavier.le-goff@univ-rennes1.fr) and DR (riveline@unistra.fr)

Acknowledgments

This work was supported by a grant for "Aide aux financements de projets innovants interdisciplines" from the SFR BIOSIT (UMS CNRS 3480 - US INSERM 018, Rennes, France) to XLG, Unistra and CNRS funds to DR. We thank J.R. Paulson and X. He (Oshkosh University, USA) for providing the NMPP1, the MRic microscopy platform for fluorescence microscopy equipment at the SFR BIOSIT (Rennes, France), F. Chang (San Francisco, USA) and V. Simanis (Lausanne, Switzerland) for strains, J. Pécreaux (IGDR, Rennes, France) and A. Trubuil (INRA, Jouy-en-Josas, France) for their help in initial image analyses and Y. Arlot-Bonnemains (IGDR, Rennes, France) for support.

References

1. Riveline, D. 2009. Explaining Lengths and Shapes of Yeast by Scaling Arguments. PLoS One. 4: e6205.

2. Tran, P.T., L. Marsh, V. Doye, S. Inoué, and F. Chang. 2001. A Mechanism for Nuclear Positioning in Fission Yeast Based on Microtubule Pushing 7. J. Cell Biol. 153: 397–411.

3. Daga, R.R., and F. Chang. 2005. Dynamic positioning of the fission yeast cell division plane. Proc. Natl. Acad. Sci. 102: 8228–8232.

4. Tatebe, H., K. Shimada, S. Uzawa, S. Morigasaki, and K. Shiozaki. 2005. Wsh3/Tea4 is a novel cell-end factor essential for bipolar distribution of tea1 and protects cell polarity under environmental stress in S. pombe. Curr. Biol. 15: 1006–1015.

5. Martin, S.G., W.H. McDonald, J.R. Yates, and F. Chang. 2005. Tea4p links microtubule plus ends with the formin for3p in the establishment of cell polarity. Dev. Cell. 8: 479–491.

6. Cadou, A., A. Couturier, C. Le Goff, T. Soto, I. Miklos, et al. 2010. Kin1 is a plasma membrane-associated kinase that regulates the cell surface in fission yeast. Mol. Microbiol. 77: 1186–1202.

bioRxiv preprint doi: https://doi.org/10.1101/520007; this version posted February 11, 2019. The copyright holder for this preprint (which was not certified by peer review) is the author/funder. All rights reserved. No reuse allowed without permission.

7. Minc, N., A. Boudaoud, and F. Chang. 2009. Mechanical Forces of Fission Yeast Growth. Curr. Biol. 19: 1096–1101.

8. Coelho, M., S.J. Lade, S. Alberti, T. Gross, and I.M. Tolić. 2014. Fusion of Protein Aggregates Facilitates Asymmetric Damage Segregation. PLoS Biol. 12: 1–11.

9. Moreno, S., A. Klar, and P. Nurse. 1991. Molecular genetic analysis of fission yeast Schizosaccharomyces pombe. Methods Enzymol. 194: 795–823.